The Effect of The E106D Mutation on HCAII

Kunlun Wang | Eric Hennemann | Addison Moran

E-mail:
kwang358@wisc.edu
akmoran3@wisc.edu
hennemann@wisc.edu

Abstract

Human carbonic anhydrase II (HCAII) is a pivotal enzyme responsible for many important body functions. Glutamic acid 106, an amino acid residue located within the active site of HCAII, plays an important role in the stability, activity, and ligand binding of the enzyme. This paper attempts to determine the effect of glutamic acid 106 to an aspartic acid mutation on the overall protein stability, enzymatic activity, and ligand binding of HCAII. Various biochemistry methods such as Gibson Assembly, protein expression, protein purification, fluorescence spectroscopy, FRET, etc. were used and we found that E106D mutation results in negligible structural disturbance, lowered enzymatic efficiency, enhanced affinity for substrate, decreased catalytic rate, enhanced ligand binding to DNSA, and decreased ligand binding to AZ. This paper presents medical implications to the ongoing medical research.

Keywords: HCAII, E106D, Gibson Assembly, protein expression, protein purification, fluorescence spectroscopy, FRET, protein stability, enzymatic activity, ligand binding.

1. Introduction

Human carbonic anhydrase II (HCAII) is one of the 16 forms of human α carbonic anhydrases and is responsible for catalyzing the reversible hydration/dehydration of carbon dioxide/bicarbonate (Avvaru et. al, 2009). It is involved in a variety of important physiological functions, such as the regulation of respiration and gas exchange, acid-base equilibria, transport of ions and fluids, and development of bone and mineralization (Sly and Hu, 1997).

Given its broad and essential role in the human body, HCAII has become a major interest for biochemists and researchers, and extensive research has been carried out to investigate its clinical relevance as a potential drug target. Particularly, HCAII has become a robust candidate to be incorporated into various novel bio-technologies such as artificial organs and biosensors (Boone et al., 2013).

This paper will study the effect of a site-directed mutagenesis of glutamic acid 106 to aspartic acid in the active site of HCAII. Glu106 is primarily responsible for 1) stabilizing the adjacent Threonine199 and 2) coordinating Zn^{2+}. The Glu106 side chain forms a (Zn^{2+})(OH^-)/Thr199/Glu106 hydrogen bond network (Marino et al., 2007) that is crucial to maintain the orientation and reactivity of the $(Zn^{2+})(OH^-)$ complex and catalysis of proton transfers.

To further understand our mutation, we visualized HCAII in Pymol and mutated Glutamic acid 106 residue to aspartic acid in the active site (Figure 1). Minimal clashes were observed, however, because aspartate's carboxylic group pointed away from Thr199, it did not coordinate Thr199 as well as glutamate which ultimately destabilized the hydroxyl group.

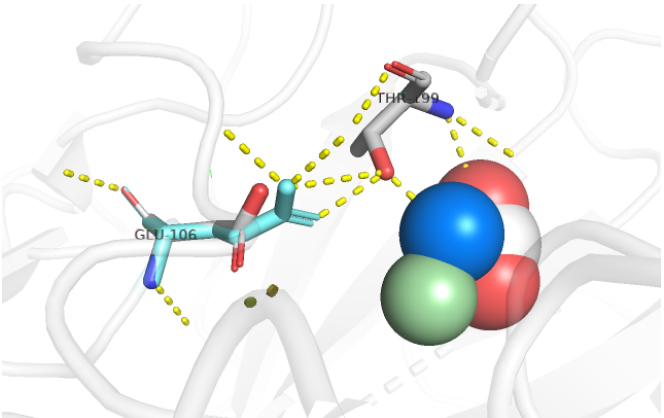

Figure 1. One conformation of the mutation of Glu106 to Asp. The original Glu106 residue is teal blue. The aspartic acid residue is

gray. CO2 are the red and gray structures in spheres. h is a green sphere and the -OH group is dark blue. Minor clashes were observed.

Based on the information we gathered in the Pymol simulations and conservation analysis, we hypothesize that because Glutamic acid 106 is completely reserved and responsible for stabilizing Threonine199, an E106D mutation will not allow for complete coordination of Thr199; this will result in a destabilized reactive hydroxyl group which will decrease enzymatic activity by preventing consistent hydration of CO2 by OH.

To test our hypothesis, first, we performed Gibson Assembly to insert the wild type HCAII gene into the pETblue2 vector. Then the Gibson assembly reactions were transformed into E. coli, screened, and successful colonies were grown in culture. DNA from the growths were purified then used to perform site-directed mutagenesis. After verification of successful mutations, the mutant DNA was transformed into E. coli.

We expressed wild type and mutant HCAII using IPTG and the T7 promoter system then purified them using affinity chromatography. Structural stability was tested by incubating the enzymes in different concentrations of urea and measuring the fluorescence after excitation at 280 nm. We tested enzymatic activity by performing a Michaelis-Menten kinetics experiment, comparing wild type and mutant esterase activities. And finally, we tested ligand binding by performing a FRET analysis using DNSA and acetazolamide (AZ).

2. Method

All experiments were performed as described in Biochemistry 551: Biochemical Methods, Fall 2020 by L Prost.

2.1 PCR Amplification of HCAII and pETblue2

In order to amplify the insert gene HCAII and the pETblue2 expression vector with primers to allow for Gibson Assembly, PCR was utilized and PCR products were run on an agarose gel to determine whether amplification resulted in the expected DNA products. For each reaction, 10 ng of template, 400 nM of the forward and reverse primers, and 1 unit of Phusion polymerase were mixed with 1x buffer, 200 μM dNTP mix, and sterile water in PCR tubes to reach a final volume of 50 uL.

The insert reaction contained insert DNA, the forward primer 5’gtttaactttaagaaggagatataccatggcccatcactgggggtacggcaaac3’ and reverse primer 5’cttaattaacattagtggtggtggtggtgtttgaaggaagctttgatttgcctgttc 3’. The vector reaction the forward primer 5’gaacaggcaaatcaaagcttccttcaaacaccaccaccaccaccactaatgttaatt aag 3’, reverse primer 5’gtttgccgtacccccagtgatgggccatggtatatctccttcttaaagttaaac 3’, and vector DNA. The negative control reaction had the insert template and the insert forward/reverse primers but did not include Phusion polymerase. All the reactions were analyzed on a 1% agarose gel.

2.2 Gibson Assembly of of HCAII into the pETblue vector and transformation of E.Coli

The DNA was prepared for Gibson assembly by adding the restriction enzyme DpnI to the amplification products. Samples were centrifuged and incubated at 37 °C for an hour. After the digests were complete, the DNA was purified using small spin columns. The Nanodrop was blanked, then used to measure the DNA concentration of the purified product with Elution Buffer. A260/A280 was calculated to determine purity; the expected A260/A280 value for pure DNA is 1.8. he DNA concentrations for the insert, vector, and negative control were 138.6 ng/uL, 62.8 ng/uL and 2.40 ng/uL respectively.

Gibson assembly was performed. Each reaction consisted of 10 uL of Gibson Assembly Master Mix, insert and vector DNA, and water was added until a final volume of 20 uL was reached. One reaction contained 0.0546 pmol vector and 0.0546 pmol insert, another contained 0.0273 pmol vector and 0.0273 pmol insert, and a control reaction contained 0.0273 pmol vector and 1.07 uL control DNA. Reactions were incubated in the thermocycler at 50℃ for 30 minutes. For transformation, 100 uL of E. coli (DH5α) and 10 uL of Gibson assembly reaction were combined. Heat shock was applied, and the E. coli were plated to LB-ampicillin-X-gal plates for screening and incubated at 37℃ overnight.

2.3 Screening for pETblue2-HCAII clones

After an overnight growth, bacteria were selected using blue/white screening and, after DNA purification, a restriction digest screen was used to differentiate positive and negative clones.

From the plate with the most colonies that were potentially positive clones (white colonies), 3 colonies were plucked, and placed into LB and ampicillin media. The cultures were incubated at 37℃ overnight.

The pure plasmid was obtained from each culture via a miniprep. The purified DNA was digested with the restriction enzyme AlwNI to differentiate positive and negative clones. A negative control (pETblue2 vector) and a positive control (pETblue2 with HCAII insert) were also digested. The total volume of each digest reaction was 10uL, which contained

0.5uL AlwNI, 1x CutSmart buffer, 100ng DNA, and water. After the digests were set up, they were spun in the nanofuge and incubated for 30 min at 37°C.

All of the digested samples are run on 1% agarose gel to determine if any of the purified samples contained the positive clones. An uncut plasmid was also run on the gel.

2.4 Expression and Purification of HCAII

After determining successful colonies for both the wild-type and E106D mutant, we expressed our proteins with the T7 promoter system under control of the Lac operon. To do this, we prepared three different growths: IPTG-treated wild type HCAII E. coli, IPTG-treated E106D mutant HCAII E. coli, and non-IPTG-treated wild type HCAII E. coli. The non-IPTG growth was used as a negative control. We incubated each growth flask at 37˚C with shaking, and at an OD600 range of 0.6 - 0.9 we collected a sample from each culture. Then we induced one wild type growth and the E106D mutant growth with IPTG to a concentration of 500uM.

After induction of IPTG we collected samples from each growth at 45, 90, and 150 minutes, along with the samples taken right before induction, and prepared them for analysis on an SDS-PAGE gel. To prepare each sample, we first centrifuged it at 4,000 rpm for 1 minute and then discarded the supernatant. We resuspended the pellet in water and added an equal volume of Denaturing buffer (tracking dye, SDS, and BME). Finally, we heated the sample to 95˚C for 10 minutes and then stored -20˚C until analysis.

After preparing the samples for analysis, we lysed the three growth cultures. First, we centrifuged the cultures at 6,000 x g for 15 minutes and discarded the supernatant. Then we added 8mL of BugBuster reagent to each culture and incubated them at room temperature for 15 minutes with minimal shaking. Next, we centrifuged our lysate at 16,000 x g for 20 minutes at 4˚C and kept the supernatant for further purification. We resuspended the pellet in 8mL water. Then we took a 10uL aliquot of the resuspension, added 20uL water and 10uL SDS sample buffer, heated that sample at 95˚C for 10 minutes, and stored in -20˚C for future analysis. And we took 10uL of supernatant and repeated the same steps to prepare for future analysis.

A nickel column was used for immobilized metal affinity chromatography to purify HCAII. Equilibration Buffer (50mM NaH2PO4, 300mM NaCl), wash buffer (50 nM NaH2PO4, 300 nM NaCl, 20 nM imidazole), and elution buffer (50 nM NaH2PO4, 300 nM NaCl, 250 nM imidazole) were used.

After chromatography, we determined concentration and purity of the eluted fractions by taking A280 and A260 readings. We calculated protein concentration using Beer-Lambert's Law (Equation 1) where C is solute concentration, A is absorbance, ε is HCAII's extinction coefficient, and l is the distance that light travels through the solution. Both wild type and E106D mutant HCAII have an extinction coefficient of 50,420 $cm^{-1}M^{-1}$. Finally, we dialyzed samples above an A280 reading of 0.3 and A260/A280 ratio lower than 0.60 in Protein Buffer (50 mM Tris, pH 7.7, 0.1 M K2SO4).

$$c = \frac{A}{\varepsilon l} \quad (1)$$

2.5 Analysis of His-tagged HCAII expression and purification

To determine if HCAII was successfully overexpressed and purified, an SDS-PAGE gel was used and the protein concentration of purified HCAII was measured. A 15% resolving gel was made with 40% acrylamide. To collect the protein, we took a 10 uL sample from the dialysis tubing, added 10 uL of SDS sample buffer, and heated the sample at 95°C for 10 minutes. Note that the A280 refers to the absorbance of the amino acid tryptophan. The blank used for measuring A280 was a protein buffer (50 mM Tris, pH 7.7, 0.1 M K2SO4). Beer's Law was then used to determine the protein concentration where ε= 50,420 $cm^{-1}M^{-1}$ (equation 1).

SDS-PAGE samples and MW markers were prepared by heating at 95°C and centrifuging. After the resolving gel was polymerized, a 4% stacking gel was made with 40% acrylamide. The gel apparatus was assembled and loaded after the stacking gel was polymerized. Gel 1 was loaded from left to right as follows: molecular weight ladder, induced wild type at 0 min, induced wild type at 60 min, induced wild type at 150 min, uninduced wild type at 0 min, uninduced wild type at 60 min, uninduced wild type 150 min, induced E106D mutant at 0 min, induced E106D mutant at 60 min, induced E106D mutant at 150 min. Gel 2 was loaded from left to right as follows (all samples were from wild type protein purification): molecular weight ladder, elution 2 (dialyzed), elution 3 (dialyzed), elution 4, wash 3, wash 5, flow through, pellet from the 20 minute spin, supernatant, final protein (dialyzed).

Gel electrophoresis was run until the dye front was at the bottom of the gel and the gel was stained using Coomassie Blue solution in order to visualize the proteins. Kimwipes were added to the staining box to draw stain out of the destain solution and the gel box was left to shake overnight. Once the gel was stained, the MW of the samples were determined by comparing the samples' relative ability (Rf) to the Rf of MW standards (equation 2).

$$R_f = \frac{Distance_{(protein\ to\ top\ of\ resolving\ gel)}}{Distance_{(dye\ front\ to\ top\ of\ resolving\ gel)}} \quad (2)$$

2.6 Determination of Protein Stability Using Chemical Denaturation and Chemical Fluorescence

To determine whether the E106D mutation affected the stability of HCAII, fluorescence spectroscopy was used to measure the fraction of unfolded protein to determine the Gibbs free energy of unfolding ($\Delta G°_{unfolding}$). To compare structural stability, we performed a protein denaturation assay and measured the fluorescence of tryptophan. In the protein denaturation assay, there were three different types of samples: blank, wild-type, and E106D mutant. Each of those samples were placed in nine conditions with urea. Across these conditions, protein concentration was kept constant. In the blank samples, there was no protein. In the wild-type and E106D mutant samples, protein concentration was 20uM. The nine conditions of urea varied in concentration and were 0, 1.0, 2.0, 3.0, 4.0, 4.5, 5.0, 5.5, 6.0, 7.0, 8.0, and 9.0 molar. Each condition of blank was made as a pair, and each condition of wild type or E106D mutant was made as triplets; the conditions were incubated at room temperature for 60-90 minutes.

Fluorescence intensity measurements were obtained by exciting at 280nm and measuring the emission from 310nm-370nm. We performed an initial analysis using Excel. The average blank intensities were subtracted from their corresponding conditions and the data was normalized by calculating the ratio of intensity at 324nm to 340nm. Data points from wild type or E106D mutant conditions with no protein were discarded. In Prism, equation 3 which relates the normalized intensities to ΔGounfolding was used to fit the data. A T-test with a significance level of 0.05 was conducted to determine if the ΔGounfolding of the wild-type and E106D mutatant were statistically different. The null hypothesis is that $\Delta G°_{unfolding}$ of wild-type and E106D mutant HCAII are the same. The alternative hypothesis is that the values of $\Delta G°_{unfolding}$ are different.

$$y = bottom + \frac{top-bottom}{1+e^{\frac{ax+dG_0}{-RT}}} \quad (3)$$

"Bottom" refers to normalized values of the fully unfolded protein, "top" is the normalized values of the fully folded protein, a is the slope of the linear relationship between urea concentration and $\Delta G°_{unfolding}$, dGo is the value determined by the fit.

The fraction of folded protein (Xf) in each condition was calculated in Excel using equation 4 to further normalize that data. The Xf values were then plotted against urea concentration. Calculation of Xf values allowed us to create a plot for determining ΔGounfolding, equation 6, by solving for Keq, equation 5.

$$Xf = \frac{(experimental\ fluorescence\ ratio - Bottom)}{Top-Bottom} \quad (4)$$

$$Keq = (Xf)^{-1} \text{ -1} \quad (5)$$

$$\Delta G°_{unfolding} = -RT \ln K_{eq} \quad (6)$$

2.7 Investigation of Enzyme Activity

Kinetic assays were performed on wild-type and E106D HCAII, measuring esterase activity, to compare kcat, KM, and catalytic efficiency. For wild-type HCAII, eight conditions of 0.07uM protein and PNPA were tested: 0.5, 1, 2, 2.5, 3, 3.5, 4, and 5mM. For E106D HCAII seven conditions of 0.1uM protein and PNPA were tested: 0.5, 0.75, 1, 2, 2.5, 3.5, and 5mM. Each reaction condition was made as triplicates. A measure of absorbance at 405nm over time was taken for each reaction, alongside a fresh blank of PNPA, at the respective concentration.

The molar absorption coefficient of PNP, the product PNPA hydrolysis, is $1.73\text{x}10^4\ M^{-1}cm^{-1}$ and was used to convert absorbance units to uM/min. The results were fitted in GraphPad Prism using the Michaelis-Menten function, Equation 7. The kcat values were calculated using equation 8, then catalytic efficiency was calculated by equation 9. Throughout the data analysis standard error was calculated.

$$V_0 = \frac{V_{max} \times [PNPA]}{K_M + [PNPA]} \quad (7)$$

$$V_{max} = K_{cat} \times [HCAII] \quad (8)$$

$$Catalytic\ Efficiency = \frac{K_{cat}}{K_M} \quad (9)$$

2.8 Performing FRET to Detect Ligand Binding to HCAII

Forster resonance energy transfer (FRET) experiments were performed on wild-type and E106D HCAII to compare the binding of DNSA and AZ. To determine the Kd for DNSA, wild-type and E106D HCAII were treated with 12 DNSA concentrations: 0, 0.05, 0.1, 0.25, 0.5, 0.75, 1, 2, 4, 6, 10, and 20 uM. To determine the Kd for AZ, wild-type and E106D HCAII were initially saturated with 20 uM DNSA and then treated with 12 AZ concentrations: 0, 0.01, 0.1, 0.25, 0.5, 0.8, 1, 2, 5, 10, 15, and 20 uM. All conditions were made in triplicates, and the final concentration of both wild-type and E106D HCAII in their respective reactions was 0.25 uM. Both DNSA and AZ FRET experiments measured DNSA binding to HCAII, therefore all conditions were excited at 280 nm and emission was measured at 470 nm.

The results for DNSA FRET experiments were analyzed by adjusting the raw fluorescence data, using equation 10, to account for the volume differences across the different conditions. The fraction saturation, r, was calculated for each data point using equation 11. Fmax is the largest adjusted fluorescence value; Fmin is the smallest adjusted fluorescence value. Using r, the concentration of free DNSA in each reaction was calculated using equation 12. To determine Kd, r and $[DNSA]_{free}$ were fitted using the Langmuir isotherm fit, equation 13, in GraphPad Prism.

$$F_{adjusted} = \frac{F_{470} \times Volume_{total}}{Volume_{initial}} \quad (10)$$

$$r = \frac{F_{adjusted} - F_{min}}{F_{max} - F_{min}} \quad (11)$$

$$[DNSA]_{free} = [DNSA]_{total} - r \times [HCAII]_{total} \quad (12)$$

$$r = \frac{[DNSA]_{free}}{K_d + [DNSA]_{free}} \quad (13)$$

The results for AZ FRET experiments were adjusted using equation 10, and r for each data point was calculated using equation 11. The concentration of free AZ was calculated using equation 14. Then the competitive Langmuir isotherm fit, equation 15, was used to determine Kd for AZ.

$$[AZ]_{free} = [AZ]_{total} - (1 - r) \times [HCAII]_{total} \quad (14)$$

$$r = \frac{1}{(1 + \frac{K_d^{DNSA}}{[DNSA]})(1 + \frac{[AZ]_{free}}{K_d^{AZ}})} \quad (15)$$

3. Results

The purpose of this study was to understand how a mutation of glutamate 106 to aspartate has an effect on HCAII's structural stability, enzymatic activity, and ligand binding affinity. After purifying both wild-type and E106D HCAII, we incubated the enzymes with uirea and determined $\Delta G°_{unfolding}$, performed kinetic assays to determine KM and kcat, and performed FRET to determine Kd for DNSA and AZ.

Protein Purification

In this experiment, we ran samples of our E. coli growths on SDS-PAGE gels to determine the success of the overexpression of wild type and E106D mutant HCAII. Figure 2 is the result of a gel used to analyze the protein expression of the growths at different time points with and without IPTG induction. In all growths two proteins are expressed much more than other proteins: HCAII and an unknown protein. In the induced wild type HCAII growth, lanes 1-3, we observed maximum expression at 150 minutes after IPTG induction. In the uninduced wild type HCAII growths, lanes 4-6, we do not observe overexpression at all. In the induced E106D HCAII, lanes 7-9, we observed maximum expression at 150 minutes after IPTG induction.

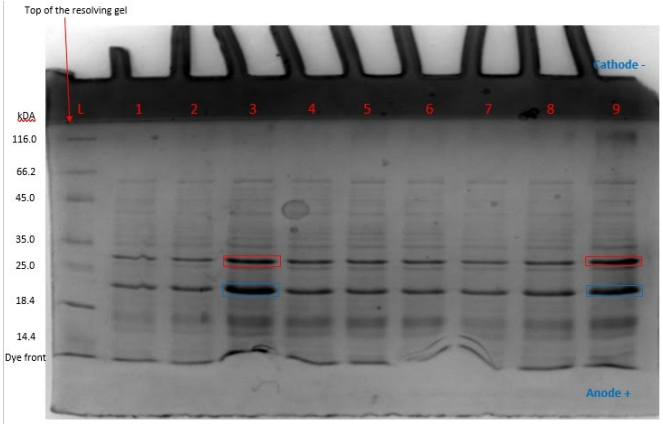

Figure 2. SDS-PAGE gel of induced wild type HCAII, uninduced wild type HCAII, and induced E106D HCAII E.Coli growths after induction with 500 uM IPTG. L is the molecular ladder; Lane 1 is wild type induced at 0 minute; Lane 2 is wild type induced at 60 minutes; Lane 3 is wild type induced at 150 minutes; Lane 4 is wild type uninduced at 0 minutes; Lane 5 is wild type uninduced at 60 minutes; Lane 6 is wild type uninduced at 150 minutes; Lane 7 is E106 D mutant induced at 0 minutes; Lane 8 is E106D induced at 60 minutes; Lane 9 is E106D mutant induced at 150 minutes. Boxed in red is the overexpression of wild type and E106D mutant. Boxed in blue is another highly expressed protein.

Figure 3 is the plot produced after we calculated the Rf values of the molecular weight ladder in figure 2and plotted them against the logarithm of the respective molecular weights. After calculating the Rf values of the two highly expressed proteins we determined that the most highly expressed protein was not HCAII. This unknown protein, boxed in blue in figure 2, has a Rf value of 0.704, which corresponds to a molecular weight of 21.912 kDa. The second most highly expressed protein, boxed in red in figure 2, has a Rf value of 0.584, which corresponds to a molecular weight of 29.189 kDa. This indicates that the protein boxed in red is HCAII.

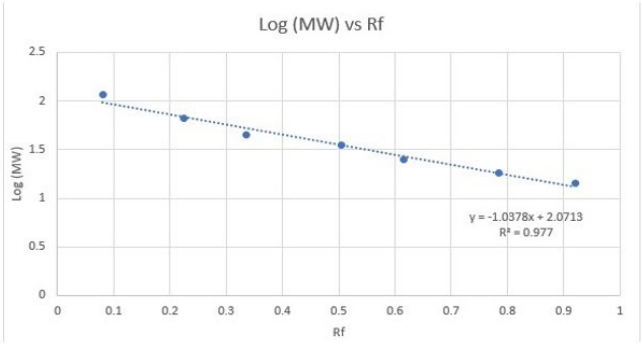

Figure 3. Molecular mass calibration curve of gel 1. Based on the R^2 value, this calibration curve is linear in the molecular weight range of 116kDa to 14.4 kDa.

Figure 4 is the result of a SDS-PAGE gel we ran to analyze purification of wild type HCAII. The eluted fractions, lanes 1-3, contained mostly HCAII with a small amount of protein contamination;lanes 1 and 2 were dialyzed, while lane 3 was not. The wash fractions, lanes 4 and 5, and the flow-through, lane 6, contained most of the other highly expressed protein. Lane 7 is the pellet of the centrifugation after growth culture cell lysis, it contains the insoluble materials. Lane 8 is the supernatant of the centrifugation after cell growth culture cell lysis, it contains the soluble materials. And the final dialyzed protein stock, lane 9, had mostly wild type HCAII. The purification was successful.

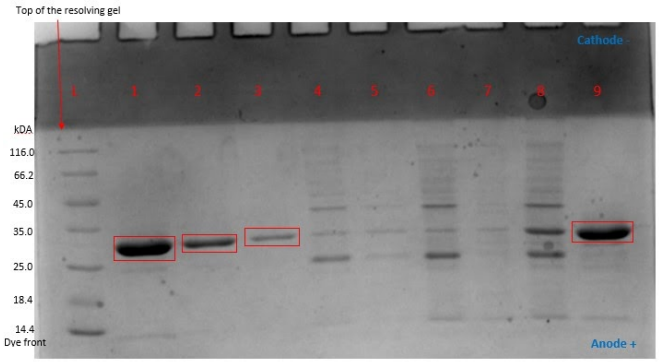

Figure 4. SDS-Page gel of samples taken during wild type HCAII purification. L is the molecular weight ladder; Lane 1 is elution fraction 2 which was dialyzed; Lane 2 is elution fraction 3 which was dialyzed; Lane 3 is elution fraction 4; Lane 4 is wash fraction 3; Lane 5 is wash fraction 5; Lane 6 is flow through; Lane 7 is the pellet of the centrifugation after growth culture cell lysis; Lane 8 is the supernatant of the centrifugation after growth culture cell lysis; Lane 9 is the final dialyzed stock of HCAII. Boxed in red is the purified wild type HCAII.

Figure 5 was produced when calculated Rf values of the molecular weight ladder in figure 4 was plotted against the logarithm of the respective molecular weights. The Rf value of the brightest band in lane 1 of figure 4 was 0.531, which corresponds to a molecular weight of 29.62 kDa. This indicates it is HCAII. The concentration of our dialyzed wild type HCAII was calculated to be 36.89 uM.

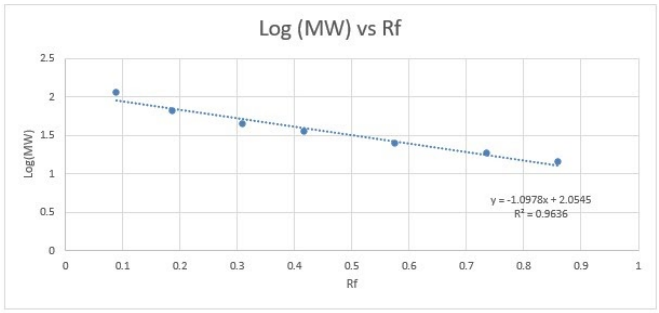

Figure 5. Molecular mass calibration curve of gel 2. Based on the R^2 value, this calibration curve is linear in the molecular weight range of 116kDa to 14.4 kDa.

Protein Stability

After ensuring that we were working with a relatively pure protein stock, we began our study of how a mutation of E106D affects HCAII by determining structural stability. To determine whether the E106D mutation affected the stability of HCAII, urea was used to denature both wild type and mutant HCAII, and fluorescence spectroscopy was used to measure the fraction of folded and unfolded HCAII.

For both wild type HCAII and E106D HCAII, fluorescence emission spectra showed a peak at roughly 324 nm which corresponds to fully folded protein (Figures 6,7). In general, proteins were fully folded at higher fluorescence and fully unfolded at lower wavelength. Fluorescence at roughly 340 nm is where all the curves cross each other, indicating that the fluorescence at this wavelength was not strongly affected by the state of the protein. Consequently, the data is normalized using the 324/340 ratio, and the 324/340 fluorescence ratio was used to measure the shift in folded to unfolded HCAII.

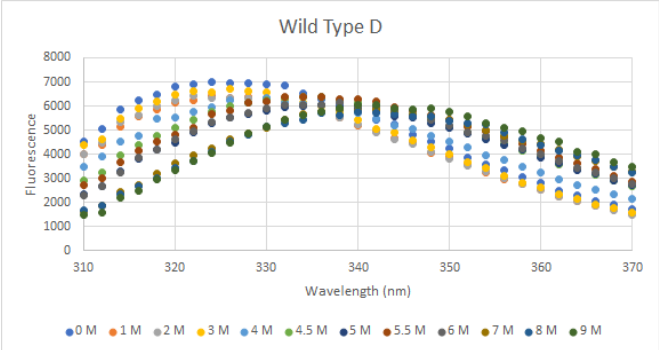

Figure 6. Emission Spectra of Wild Type HCAII after urea denaturation. Wild type HCAII was incubated with urea at the indicated concentrations of urea (M). Tryptophans were excited at 280 nm and fluorescence emission was measured from 310 to 370 nm. Sample D is shown.

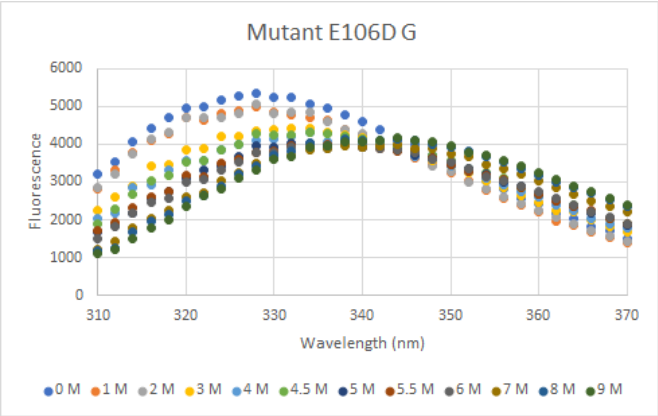

Figure 7. Emission Spectra of E106D HCAII after urea denaturation. E106D HCAII was incubated with urea at the indicated concentrations of urea (M). Tryptophans were excited at 280 nm and fluorescence emission was measured from 310 to 370 nm. Sample G is shown.

Because there is a logarithmic relationship between $\Delta G°_{unfolding}$ and Xf, the plot for Xf was sigmoidal (Figure 8). There are small differences in the curves for the wildtype and mutant HCAII. Between urea concentrations of 0- 3 M, the wild type protein has an Xf that is closer to 1, indicating that is more folded relative to E106D HCAII. The two curves are the same between urea concentrations of 4- 6 M. Between urea concentrations of 7-9 M, the wild type protein has an Xf that is closer to 0, indicating it is more unfolded relative to E106D HCAII. The standard error for both wild type and mutant samples were small.

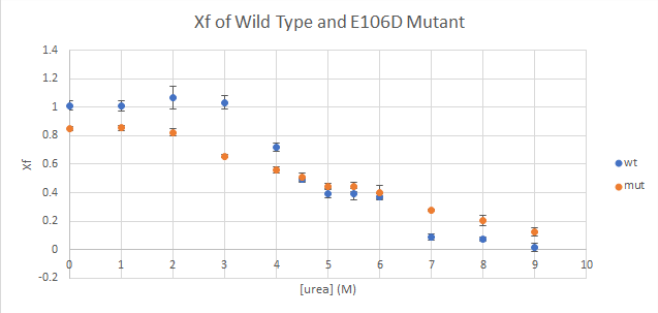

Figure 8. Plot of Xf and against urea concentration of wild type HCAII and HCAII E106D. Xf represents the fraction of folded protein at each urea concentration. The average Xf at each urea concentration was taken for both the wild type and mutant. Error bars are the standard deviation of the wild type and mutant samples. At roughly 1, the protein is fully folded and, at roughly 0, the protein is fully unfolded.

$\Delta G°_{unfolding}$ was determined from Xf and Keq of the wild type and mutant HCAII. Because some values of Keq were negative, the $\Delta G°_{unfolding}$ for some urea concentrations of wild type HCAII could not be calculated. Both the curves for wild type HCAII and E106D HCAII are roughly linear, and the wild type curve has a larger slope than the mutant curve (Figure 9). Similar to the graph of Xf, between urea concentrations of 0-4 M, the wild type has a larger positive $\Delta G°_{unfolding}$, indicating that folding is more favorable for the wild type than the mutant. The curves are the same between 4.5- 6 M. Between 7-8 M urea, the wild type has more negative $\Delta G°_{unfolding}$, indicating that protein unfolding of the wild type is more favorable than protein unfolding for the mutant. The apparent Cm appears at 4.5 M urea.

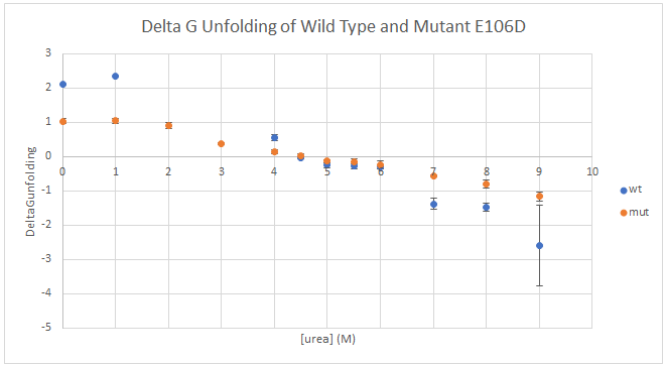

Figure 9. Plot Of delta G unfolded of wild type HCAII and HCAII E106D against urea concentration. The average delta G unfolded at each urea concentration was taken for both the wild type and mutant. Error bars represent the standard deviation of the wild type and mutant samples. The equation for the plot of delta G unfolded for wild type HCAII is y = -0.5333x + 2.5406 (R=0.966) and the equation for the mutant plot is y = -0.2546x + 1.2094 (R=0.9797). At low urea concentrations, delta G unfolded is positive and folding is favored. At high urea concentrations, delta G unfolded is negative and unfolding is favored.

Cm is the denaturant concentration where half of the protein is folded and half of the protein is unfolded, or where the folded and unfolded states are in equilibrium (Munoz and Sanchez-Ruiz, 2004). The y-intercept from the plot of $\Delta G°_{unfolding}$ for wild type HCAII was 2.5406 and the y-intercept for the mutant plot was 1.2094, which was expected to correlate to the $\Delta G°_{unfolding}$ values determined by Prism (Table 1). The y-intercepts of the plots for $\Delta G°_{unfolding}$ for both the wild-type and mutant HCAII were similar to the $\Delta G°_{unfolding}$ values predicted by Prism.

Table 1. Prism data analysis determination of Cm and $\Delta G°_{unfolding}$. A prism analysis of the 324/340 fluorescence ratios for wild type HCAII and HCAII E106D was used to determine Cm and $\Delta G°_{unfolding}$ for each data set. The standard error of $\Delta G°_{unfolding}$ and the 95% confidence interval for Cm for each data set is reported. Note: there was an error in the prism analysis so the standard error of Cm could not be reported.

	$\Delta G_{unfolding}$	Standard Error $\Delta G_{unfolding}$	C_m	95% CI (asymptotic) C_m
Wild-Type	2.514	1.011	4.878	4.338 to 5.048
Mutant E106D	1.203	0.2475	4.753	4.581 to 4.924

The p-value is 0.1965 so we do not reject the null hypothesis (including outliers); there is no statistical difference between the $\Delta G°_{unfolding}$ values of wild-type and E106D HCAII.

Enzymatic Activity

The esterase activity of HCAII on 4-nitrophenyl acetate (PNPA) was used to perform a kinetic assay in order to determine kcat, KM and the overall catalytic efficiency for both wild type HCAII and E106D HCAII; this comparison was done to determine if an E106D mutation has an effect on the catalytic activity of HCAII.

The KM for wild type HCAII is approximately 3 times larger than that of the E106D (Figure 10). The p-value for comparing the KM of each data set is <0.0001. Vmax for wild type HCAII is much larger than that of the E106D, however comparing the Vmax values is not effective in this case because the enzyme concentration in the assays were different. The kcat for wild-type HCAII is approximately 5 times greater than that of the E106D. Ultimately this results in the wild-type having an approximately 50% greater catalytic efficiency than the E106D (Table 2).

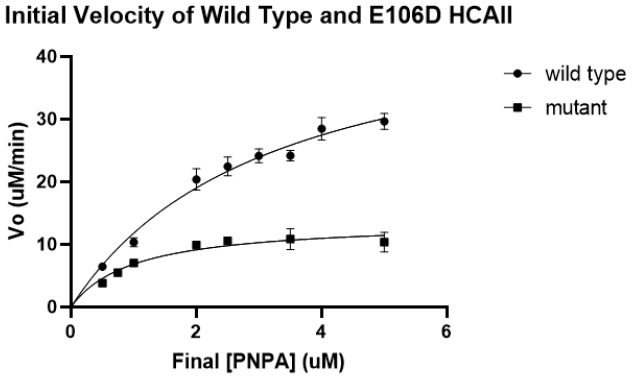

Figure 10. Plot of Vo vs. [S] for Wild Type and E106D HCAII from Prism. Vo was determined experimentally using a dual-beam spectrophotometer and plotted against the final substrate concentration to compare the esterase activity of wild type HCAII to mutant HCAII.

Table 2. Table of Km, Kcat, and Kcat/Km for wild type and E106D HCAII. Kcat and Kcat/Km were calculated using Vmax and Km values provided by Prism data analysis. Vmax and Km standard error was provided by Prism data analysis. Error was propagated throughout calculations of Kcat and Kcat/Km to determine the absolute error of each value per data set.

	Km (uM)	Km standard error (uM)	Kcat (min^{-1})	Kcat absolute error (min^{-1})	Kcat/Km ($M^{-1}min^{-1}$)	Kcat/Km absolute error ($M^{-1}min^{-1}$)
Wild Type HCAII	3.184	0.4682	704.7	52	221.3	48.88
E106D HCAII	1.005	0.1941	137.2	8.871	136.5	35.19

Ligand Binding

After analyzing the catalytic effect the E106D mutation had on HCAII, FRET was used to detect ligand binding of DNSA to wild type and E106D HCAII, and competition between DNSA and AZ was used to find the Kd of AZ to determine the overall effect E106D had on ligand binding to HCAII.

The Langmuir Isotherm plots for the binding of DNSA to wild type and E106D HCAII were hyperbolic (Figure 10). The wild type and E106D HCAII appeared to have similar Kd values based on the plots, with a difference of roughly 0.16 uM^{-1} (Table 3). The p-value determined by a Prism analysis between the two datasets was 0.0034.

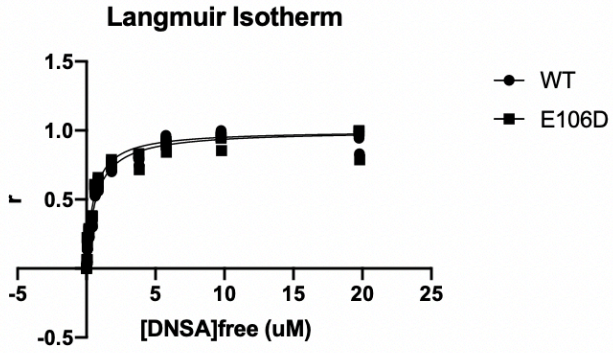

Figure 11. Langmuir Isotherm plot of the fraction of saturation, r, against $[DNSA]_{free}$. Fluorescence emission was measured at 470 nm at various DNSA concentrations and used to determine r.

Table 3. Table of Kd DNSA and Kd AZ values for wild type and E106D HCAII. A Prism analysis was run using Kd of DNSA, fraction saturation r and $[AZ]_{free}$ to determine Kd of AZ.

	K_d (uM^{-1})	Std. Error of K_d (uM^{-1})	K_d AZ (nM^{-1})	Std. Error K_d AZ (nM^{-1})
Wild type	0.6811	0.03650	3.851	0.7574
E106D	0.5186	0.03654	6.468	0.5924

The Kd AZ for E106D was roughly 1.5 times the value of Kd AZ for the wild type (Table 3). The p-value determined by a Prism analysis between the two datasets was 0.0179.

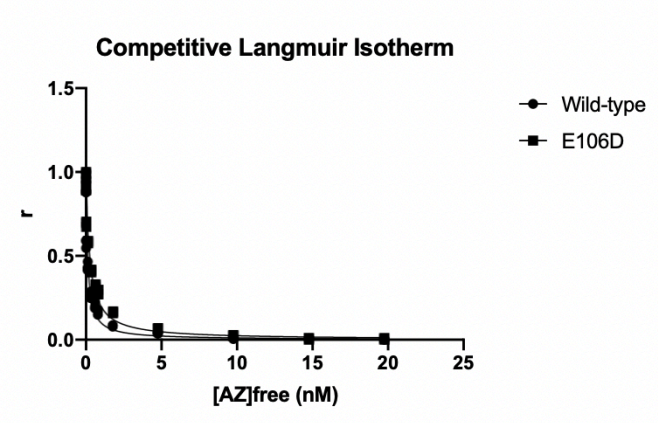

Figure 12. Competitive Langmuir Isotherm plot of fraction saturation, r, against $[AZ]_{free}$ for wild type and E106D HCAII. Fluorescence emission was measured at 470 nm at various AZ concentrations based on AZ competition with DNSA.

4. Discussion

Protein Purification

Using SDS-PAGE to measure the protein concentration of HCAII allowed us to determine if HCAII was successfully expressed and purified. In order to fully analyze our expression and purification, we ran two SDS-PAGE gels. The first gel contained induced wild type HCAII, uninduced wild type HCAII, and induced mutant HCAII (figure 2). The main purpose of this gel was to indicate whether HCAII expression was induced in the E.coli system. We expected to see overexpression of HCAII after induction with IPTG. We observed that after induction with IPTG, there was a gradual boldening of the protein bands over the different time points. This is an indication that HCAII overexpression was successful.

The second gel contains samples that were collected in the process of immobilized metal affinity chromatography, using a nickel column (Figure 4). The main goal of the second gel was to monitor the status of the purification procedure and determine whether HCAII was successfully purified through the nickel column. We expected to see that after the nickel column purification, we only retained the HCAII proteins. The HCAII samples are efficiently purified, as indicated by the single bolden clear band of the elution sample in our dialyzed stock in lane 9.

For both wild-type and E106D HCAII, two proteins are highly expressed, including HCAII (29.189 kDa) and an unknown protein (21.912 kDa). This unknown protein is present in similar concentrations to HCAII in the uninduced wild type HCAII growth, and it seems to follow the same expression patterns of both wild type and E106D HCAII (figure 2). However, this protein is most likely an endogenous E. coli protein naturally expressed in large quantities.

The HCAII protein was successfully purified since all the elution fractions contain HCAII with only a small amount of protein contamination (Figure 4, lanes 1, 2, and 3), and the final dialyzed protein stock mainly has wild-type HCAII protein (Figure 4, lane 9). Conversely, the wash fractions (lanes 4 and 5) and the flow-through (lane 6) contain the other unknown protein (figure 4). Because the wash fractions and flow-through contain the other unknown protein, we can conclude that the unknown protein was successfully removed from the column with a buffer containing a low concentration of imidazole. Furthermore, because mostly HCAII is present in the selected elution fractions (based on the 260/280 ratios), this indicates that HCAII was successfully eluted with a higher concentration of imidazole. The presence of pure HCAII is further confirmed because a band corresponding to HCAII on the gel appears in the final dialyzed protein stock, which was used to remove salt and small molecules such as imidazole.

To further purify our HCAII stocks, we can perform ligand affinity chromatography. Because HCAII and the unknown protein have similar molecular weights, it wouldn't make sense to separate the protein by size. Because affinity chromatography is based on the selective binding affinity of a protein for a ligand, HCAII can be selected for by using DNSA. HCAII will bind to the immobilized ligand and contaminated proteins will be washed from the column using a low concentration of the soluble version of the ligand. HCAII will be eluted using a higher concentration of the soluble ligand.

Protein Stability

After successfully purifying wild-type and E106D HCAII, we began our comparative study with protein stability by experimentally determining the Gibbs free energy of unfolding ($\Delta G°_{unfolding}$). Wild-type and E106D HCAII were incubated with urea, 0 M to 9M, and the fluorescence of tryptophan was measured. The midpoint concentration of unfolding (Cm) was 4.878 M urea for wild-type HCAII with a 95% confidence interval from 4.338 M to 5.048 M urea, and 4.783 M urea for HCAII E106D with a 95% confidence interval from 4.581 M to 4.924 M urea (Table 1). In a study done by Boren et.al (2004), Cm of wild-type HCAII incubated with urea to be 4.4 M. This published data lies within the 95% confidence interval of the Cm extrapolated from our experimental data for wild-type HCAII. Therefore, it is likely that the correct Cm of urea for wild-type HCAII is within our confidence interval.

The $\Delta G°_{unfolding}$ of the wild-type HCAII obtained from the experiment is 2.5141.011 (Table 1). According to Wahiduzzaman et.al (2017), the $\Delta G°_{unfolding}$ change associated with HCAII changing from its native folded state to unfolded denatured state is 8.54 kcal/mol. Our $\Delta G°_{unfolding}$ data is significantly different from this published source but our experimental conditions were similar. Wahiduzzaman et.al used a 50mM tris-HCl buffer, pH 7.5, at 25oC; we used Protein Buffer, which has a pH of 7.7 and contains a 50mM tris and 0.1 M K2SO4, at 25oC. Since pH can affect protein kinetics and therefore protein denaturation, it might be possible that the difference in $\Delta G°_{unfolding}$ is due to differences in pH. However, the pH difference here is very small so it is more likely that a major difference occurred in how we collected data. Wahiduzzaman et.al measured optical activity, and calculated $\Delta G°_{unfolding}$ for the transition to the first intermediate, second intermediate, and fully denatured protein. We measured the fluorescence of tryptophan from 310nm to 370nm, and calculated $\Delta G°_{unfolding}$ using the ΔG fit, equation 3. Therefore, our different methods of determining $\Delta G°_{unfolding}$ most likely resulted in the large discrepancy between our value and Wahiduzzaman et.al.

The largest abnormality in the data appears in the standard error for the $\Delta G°_{unfolding}$ plot of the wild type HCAII at 9 M urea. This is due to a large $\Delta G°_{unfolding}$ from one data point in the triplicate, even though no obvious abnormalities are apparent in the emission spectrum.

Our experimental data indicates that the $\Delta G°_{unfolding}$ of the E106D is 1.2030.2475 kcal/mol which is much smaller than that of its wild-type counterpart, which is 2.5141.011 kcal/mol (Table 1). Therefore, E106D HCAII is less favored towards folding and more favored towards unfolding compared to its wild-type. However, the $\Delta G°_{unfolding}$ of the wild-type and E106D HCAII are not statistically significant; a subtle change in $\Delta G°_{unfolding}$ is not enough to substantially change the percentage of unfolded proteins in the sample, which is confirmed by the p-value calculated in the result section. Therefore, we extrapolate that the E106D mutation does not appear to significantly affect the structural stability of HCAII, statistically. In a biological standpoint, however, HCAII wild type and E106D mutant might be biologically different. With HCAII wild type being more stable thermodynamically compared to the E106D mutant, the mutant's protein kinetics and enzymatic activities might be negatively affected by its unfolding effect.

Future studies of HCAII structural stability should follow a protocol similar to Wahiduzzaman et.al. We should employ a method such as circular dichroism as a way to confirm if the $\Delta G°_{unfolding}$ values we obtained by measuring tryptophan fluorescence is correct.

Enzymatic Activity

After comparing $\Delta G°_{unfolding}$ of the wild-type and mutant to access HCAII structural stability, kcat/KM (catalytic efficiency) was used to determine how efficiently HCAII converts PNPA to PNP. The catalytic efficiency for wild-type HCAII was approximately 221.3 $M^{-1}Min^{-1}$ and the catalytic efficiency for E106D HCAII was approximately 136.5 $M^{-1}Min^{-1}$ (Table 2). The catalytic efficiency of E106D HCAII was lower than that of wild type HCAII, therefore it has a lower enzymatic activity.

The KM value for E106D HCAII was significantly and statistically lower than its wild-type counterpart, indicating that E106D HCAII had a slightly stronger affinity for the PNPA than the wild-type HCAII. The wild-type HCAII had a kcat value of approximately 704.7Min^{-1}which is significantly higher than the kcat value of the E106D HCAII, which was approximately137.2 Min^{-1}. Because the wild-type had a higher kcat, the wild-type is much more efficient at turning over PNPA.The Vmax value for the wild-type was approximately 49.33 uM/min which is much higher than that of the E106D HCAII which was approximately 13.72 uM/min. However, in this case it is not valid to directly compare the Vmax values because the concentrations of wild-type and E106D HCAII were not equal in the assays.

Based on the values of the kinetic parameters obtained, E106D HCAII has a larger affinity for PNPA, however, this advantage is compromised by the drastic decrease in its catalytic rate, resulting in an overall decrease in catalytic efficiency. This is consistent with the structural and biochemical properties of the mutation. The mutation of Glu106 to Asp106 results in minimal structural clashes with the neighboring environment and no polarity change, and because Asp is slightly smaller in size than Glu, the mutation results in slightly larger hydrophobic pocket size of the HCAII enzyme. According to Höst et.al (2006), an increased size of the hydrophobic pocket can result in increased activities and specificities for longer substrates such as PNPA. Therefore, the increase in KM in E106D of HCAII can be rationalized by the increase in size of the hydrophobic pocket of HCAII such that larger substrates such as PNPA can more easily bind and stay in the pocket.

Based on the pyMol analysis on the effect of E106D on DNSA ligand binding conducted previously, minimal adverse effects were observed upon the mutation, which further reinforces the favorable effect of the E106D mutation on ligand binding (smaller KM). The catalytic ability of HCAII, however, is compromised by the E106D mutation, using

pyMol mutagenesis tool, we observed potential destabilizing factors, specifically, destabilization of the (Zn^{2+})(OH^{-})(Thr199)(Glu/Asp106) hydrogen bond network which is pivotal for enzymatic activities. Such local disturbance might propagate to negatively affect the catalysis of the ligand, which will result in significant reduction in kcat. Overall, the catalytic destruction will prevail and lead to a salient decrease in kcat/KM.

In the future, to improve this experiment, studies should consider adding a few more substrate concentrations. In the Michaelis Menten diagram we obtained, the wild-type HCAII didn't seem to reach the final plateau area, so in order to have a good fit of Km and Vmax, we need to add a few more reactions of higher substrate concentration. Second, PNPA, which is the substrate used in this experiment, experiences self-hydrolysis in an aqueous buffer solution. Even though we included a blank sample to measure the amount of the yield that is not due to the effect of HCAII enzyme, the most accurate solution is to employ a non-self-hydrolysable ester such as 2-naphthyl acetate (2NA), which is also an ester that HCAII can hydrolyze, according to Gould and Tawfik (2005). The hydrolysis of 2NA produces acetate and 2-naphthol, which absorbs light at 320nm (He, 2003). We can do a similar assay, measuring the continuous formation of 2-naphthol in a spectrophotometer. One caveat is that the catalytic efficiency of HCAII with 2NA is 82 times lower than HCAII with PNPA(Gould and Tawfik, 2005). However, this should not be an issue since we're only interested in comparing the enzymatic activity of wild-type and E106D HCAII.

Overall, the E106D mutation decreased catalytic activity of HCAII. In the next experiment, we used FRET to determine the effect the E106D mutation has on ligand binding.

Ligand Binding

After determining the effect of E106D mutation on enzymatic activities, HCAII's ligand binding was assessed using FRET. The experimental data suggests that the E106D mutation results in slightly stronger binding affinity for DNSA and mildly reduced binding affinity for AZ. Structurally, both DNSA and AZ are sulfonamide molecules with a -SO2NH2 group attached on a ring structure. And according to Boriack-Sjodin et.al (1998), the primary interactions between the HCAII active site and the sulfonamide compounds is the coordination of the primary sulfonamide group to the active site zinc ion; the ionized sulfonamide nitrogen is able to displace the hydroxide bound to the zinc ion and form a very stable tetrahedral enzyme-sulfonamide complex geometry with extraordinary binding affinities. Moreover, according to Chen and Kernohan (1969), the effectiveness of a sulfonamide binding is associated with the ease with which a proton can dissociate from the sulfonamide group, as a proton from the sulfonamide group can form hydrogen bond with the oxygen atom of the Thr199 residue of the HCAII active site. This means that the more acidic the sulfonamide is, the more potent it is as an inhibitor. AZ has a pKa of 7.2 and DNSA has a pKa of 9.97, therefore, AZ is much more acidic than DNSA meaning that it will bind with HCAII more strongly. The experimental Kd values obtained for the wild-type HCAII are in agreement with K_d^{DNSA} = 0.2 0.1 uM and K_d^{AZ} = 6 3 nM reported by Wang & Zamble (2006), however, the experimental Kd values for the E106D differ from the K_d^{DNSA} = 0.2 uM and K_d^{AZ} = 4 nM. This discrepancy could arise from a variety of reasons such as the difference in salt concentration, temperature, and pH, according to Jarmoskaite et.al (2020).

One reason DNSA has increased binding affinity to HCAII after the E106D mutation is due to the size. Aspartic acid is slightly smaller compared to glutamic acid. An increased size of the hydrophobic pocket can result in increased activities and specificities and less steric interactions for larger substrates like DNSA (Höst et.al, 2006).

The pka change could also increase the binding affinity of DNSA to HCAII in E106D. Both the pKa -carboxyl group (pKa = 1.88) and the -ammonium ion (pKa = 9.60) of aspartic acid has a slightly lower pKa than that of the glutamic acid (with -carboxyl group pKa = 2.19 and -ammonium ion pKa = 9.67). According to Nair et.al (1995), changing from Glutamic acid to Aspartic acid would alter the pKa of the zinc-water complex, which ultimately alters the pH dependency of the sulfonamide binding to HCAII, therefore, favoring DNSA binding to HCAII.

A destabilized hydroxyl group could also cause DNSA to have increased binding affinity to HCAII after the mutation. The E106D mutation resulted in a destabilized hydroxyl group, and this makes it easier for the ionized nitrogen of DNSA to displace the hydroxyl group. And since DNSA binds tighter to HCAII's active site, it makes it even more difficult for AZ to compete to displace the DNSA. Therefore, a decrease in AZ binding was observed after the mutation. From a biological standpoint, E106D mutation decreases the efficiency of AZ as an HCAII inhibitor. This might have medical implications as AZ is a medication for various diseases and conditions.

A conformational change could occur upon DNSA or AZ binding which could have an effect on the Kd values. Therefore, in order to understand the extent of conformational change upon DNSA/AZ binding, a protein crystallography experiment could be conducted and the electron density map produced could be used to investigate the scale of conformational change. Furthermore, it is still unknown

whether E106D mutation would affect physical properties of HCAII such as its melting temperature. A DSF assay could be used to monitor the thermally induced protein denaturation.

Acknowledgements

We want to thank Prof. Lynne Prost and TAs Raghav and Hugo for their help on our experimental procedures, data collection, and data analysis.

References

[1] Avvaru, B. S., Busby, S. A., Chalmers, M. J., Griffin, P. R., Venkatakrishnan, B., Agbandje Mckenna, M., . . . Mckenna, R. (2009). Apo-Human Carbonic Anhydrase II Revisited: Implications of the Loss of a Metal in Protein Structure, Stability, and Solvent Network,. *Biochemistry, 48*(31), 7365-7372. doi:10.1021/bi9007512

[2] Borén, K., Grankvist, H., Hammarström, P., & Carlsson, U. (2004). Reshaping the folding energy landscape by chloride salt: Impact on molten-globule formation and aggregation behavior of carbonic anhydrase. *FEBS Letters, 566*(1-3), 95-99. doi:10.1016/j.febslet.2004.03.105

[3] Boone, C., Habibzadegan, A., Gill, S., & Mckenna, R. (2013). Carbonic Anhydrases and Their Biotechnological Applications. *Biomolecules, 3*(4), 553-562. doi:10.3390/biom3030553

[4] Marino, S., Hayakawa, K., Hatada, K., Benfatto, M., Rizzello, A., Maffia, M., & Bubacco, L. (2007). Structural Features that Govern Enzymatic Activity in Carbonic Anhydrase from a Low-Temperature Adapted Fish, Chionodraco hamatus. *Biophysical Journal, 93*(8), 2781-2790. doi:10.1529/biophysj.107.107540

[5] Munoz, V., Sanchez-Ruiz, M. (2004). Exploring Protein Folding Ensambles: A Variable-barrier Model for the Analysis of Equilibrium Unfolding Experiments. *PNAS*, 101 (51): 17646-17651. doi: 10.1073/pnas.0405829101

[6] Prost, L. 2020. Biochemical Methods Laboratory Manual.

[7] Sly, W. S., & Hu, P. Y. 1995. Human carbonic anhydrases and carbonic anhydrase deficiencies. *Annual review of biochemistry*, *64*(1), 375-401.

[8] Wahiduzzaman, Dar, M. A., Haque, M. A., Idrees, D., Hassan, M. I., Islam, A., & Ahmad, F. (2017). Characterization of folding intermediates during urea-induced denaturation of human carbonic anhydrase II. *International Journal of Biological Macromolecules, 95*, 881-887. doi:10.1016/j.ijbiomac.2016.10.073

[9] Krishnamurthy, V. M., Kaufman, G. K., Urach, A. R., Gitlin, I., Gudiksen, K. L., Weibel, D. B., & Whitesides, G. M. (2008). ChemInform Abstract: Carbonic Anhydrase as a Model for Biophysical and Physical-Organic Studies of Proteins and Protein-Ligand Binding. *ChemInform, 39*(24). doi:10.1002/chin.200824266

[10] Wang, S. C., & Zamble, D. B. (2006). Fluorescence analysis of sulfonamide binding to carbonic anhydrase. Biochemistry and Molecular Biology Education, 34(5), 364-368. doi:10.1002/bmb.2006.494034052656

[11] Jarmoskaite, I., AlSadhan, I., Vaidyanathan, P. P., & Herschlag, D. (2020). How to measure and evaluate binding affinities. *ELife*, *9*, 1–34. https://doi.org/10.7554/elife.57264

[12] Nair, S. K., Krebs, J. F., Christianson, D. W., & Fierke, C. A. (1995). Structural basis of inhibitor affinity to variants of human carbonic anhydrase II. *Biochemistry*, *34*(12), 3981–3989. https://doi.org/10.1021/bi00012a016

[13] Boriack-Sjodin, P. A., Zeitlin, S., Christianson, D. W., Chen, H.-H., Crenshaw, L., Gross, S., Dantanarayana, A., Delgado, P., May, J. A., & Dean, T. (1998). Structural analysis of inhibitor binding to human carbonic anhydrase II. *Protein Science*, *7*(12), 2483–2489. https://doi.org/10.1002/pro.5560071201

[14] R. F. Chen, J. C. Kernohan (1967) Combination of bovine carbonic anhydrase with a fluorescent sulfonamide, J. Biol. Chem. 242, 5813–5823.